Journal of Dental Research
2018, Vol. 97(2) 209–217

DOI: 10.1177/0022034517729811
journals.sagepub.com/home/jdr

Expression of Phosphate Transporters during Dental Mineralization

L. Merametdjian[1,2,3], S. Beck-Cormier[1,2], N. Bon[1,2], G. Couasnay[1,2], S. Sourice[1,2], J. Guicheux[1,2,3], C. Gaucher[4,5*], and L. Beck[1,2*]

Abstract

The importance of phosphate (Pi) as an essential component of hydroxyapatite crystals suggests a key role for membrane proteins controlling Pi uptake during mineralization in the tooth. To clarify the involvement of the currently known Pi transporters (Slc17a1, Slc34a1, Slc34a2, Slc34a3, Slc20a1, Slc20a2, and Xpr1) during tooth development and mineralization, we determined their spatiotemporal expression in murine tooth germs from embryonic day 14.5 to postnatal day 15 and in human dental samples from Nolla stages 6 to 9. Using real-time polymerase chain reaction, in situ hybridization, immunohistochemistry, and X-gal staining, we showed that the expression of *Slc17a1, Slc34a1*, and *Slc34a3* in tooth germs from C57BL/6 mice were very low. In contrast, *Slc34a2, Slc20a1, Slc20a2*, and *Xpr1* were highly expressed, mostly during the postnatal stages. The expression of *Slc20a2* was 2- to 10-fold higher than the other transporters. Comparable results were obtained in human tooth germs. In mice, *Slc34a2* and *Slc20a1* were predominantly expressed in ameloblasts but not odontoblasts, while *Slc20a2* was detected neither in ameloblasts nor in odontoblasts. Rather, *Slc20a2* was highly expressed in the stratum intermedium and the subodontoblastic cell layer. Although *Slc20a2* knockout mice did not show enamel defects, mutant mice showed a disrupted dentin mineralization, displaying unmerged calcospherites at the mineralization front. This latter phenotypical finding raises the possibility that Slc20a2 may play an indirect role in regulating the extracellular Pi availability for mineralizing cells rather than a direct role in mediating Pi transport through mineralizing plasma cell membranes. By documenting the spatiotemporal expression of Pi transporters in the tooth, our data support the possibility that the currently known Pi transporters may be dispensable for the initiation of dental mineralization and may rather be involved later during the tooth mineralization scheme.

Keywords: phosphate transport proteins, odontogenesis, tooth calcification/genetics, gene expression, knockout mice, Slc20a2 protein

Introduction

During mineralization of bone and dentin, the mechanism resulting in the nucleation of carbonate-substituted hydroxyapatite crystals and their deposition within the extracellular matrix is still a matter of vigorous debate (Boonrungsiman et al. 2012). Early mineral deposition can arise through the budding of matrix vesicles from the plasma membrane, which will serve as sites for calcium and phosphate (Pi) accumulation to initiate the deposition of apatite crystals (Millán 2013). The formation of hydroxyapatite crystals can also occur from solution by charged noncollagenous proteins in the collagen spaces or from a transient amorphous mineral precursor deposited within the collagen gap zones (Boonrungsiman et al. 2012; Habraken et al. 2013; Veis and Dorvee 2013). These mechanisms are not mutually exclusive and may represent redundant or additional processes to ensure proper mineralization. In all cases, the availability of Pi to form hydroxyapatite crystals is a critical factor for proper mineralization. The plasma Pi concentration but also the intracellular and extracellular Pi concentrations in the vicinity of mineralizing cells therefore represent essential parameters of the mineralization process. Despite this importance, the mechanisms by which Pi is translocated from the serum to the mineralization site are still poorly understood. It is hypothesized that Pi uptake by mineralizing cells is a prerequirement to the mineralization process and that expression and activity of Pi transporters in mineralizing cells play a central role.

In mammals, Pi uptake is mediated by high-affinity and low-capacity sodium-dependent Pi transporters that are grouped in 3 dissimilar families (Forster et al. 2011). The SLC17 family is mainly represented by Npt1/Slc17a1, a voltage-dependent polyspecific anion (including Pi) transporter (Reimer 2013). Its role in mineralization is not documented. The SLC34 family gathers Npt2a/Slc34a1, Npt2b/Slc34a2, and Npt2c/Slc34a3. The analysis of *Slc34a1* expression gave conflicting results,

[1]INSERM, U1229, RMeS, Nantes, France
[2]Université de Nantes, UMR_S1229, UFR Odontologie, Nantes, France
[3]CHU Nantes, PHU 4 OTONN, Nantes, France
[4]Dental School, University Paris Descartes, PRES Sorbonne Paris Cité, Montrouge, France
[5]AP-HP, Odontology Department, Hôpital Albert Chenevier, GHHM, Créteil, France
*Authors contributing equally to this article.

A supplemental appendix to this article is available online.

Corresponding Author:
L. Beck, INSERM U1229-RMeS, Faculté de Chirurgie Dentaire, 1 place Alexis Ricordeau, 44042 Nantes cedex 1, France.
Email: laurent.beck@inserm.fr

being reported in mineralizing rat pulpal cell line 1 (MRPC-1; Lundquist et al. 2002) but not in primary human pulp cells differentiated into odontoblasts and M2H4 and ALC cells (Tada et al. 2011; Merametdjian et al. 2016) nor in murine dental germs or whole rat incisors (Onishi et al. 2007; Yoshioka et al. 2011). Similar results were obtained for *Slc34a3*, which is not expressed in dental tissues, at least in rodents (Onishi et al. 2007; Yoshioka et al. 2011; Merametdjian et al. 2016). In contrast, Slc34a2 was expressed in MRPC-1 cells (Lundquist et al. 2002), murine dental germs, secretory and mature ameloblasts, and differentiated odontoblasts (Onishi et al. 2007). Expression of SLC20 family members PiT1/SLC20a1 and PiT2/SLC20a2 was detected in primary human pulp cells differentiated into odontoblasts (Tada et al. 2011), MRPC-1 (Lundquist et al. 2002), MO6-G3 odontoblasts (Wittrant et al. 2009; Bourgine et al. 2011), and M2H4 and ALC cell lines (Merametdjian et al. 2016). *Slc20a2* was also shown to be mostly expressed in the pulp mesenchyme and in ameloblasts during murine dental development (Zhao et al. 2006). Interestingly, the International Mouse Phenotyping consortium reported changes in the incisor color of *Slc20a2*$^{-/-}$ mice and skeletal abnormalities (http://www.mousephenotype.org/data/search/gene?kw=%22Slc20a2%22).

When trying to infer the putative role of Pi transporters in dental mineralization from the available data, one should bear in mind the diversity of the in vitro cell models used and the fact that they cannot be representative of the accurate spatiotemporal scheme of epithelial-mesenchymal interactions leading to odontogenesis. The diversity of the experimental models and technical approaches, the different time scales used, and the absence of a systematic approach make any comparison among the transporters precarious. Hence, to better assess the involvement of Pi transporters in dental mineralization, we investigated their spatiotemporal expression during tooth development and mineralization in vivo in mouse tooth germs from embryonic day 14.5 (E14.5) to postnatal day 15 (P15) and in human dental samples from Nolla stages 6 to 9. We also assessed the histologic phenotype of the tooth from mice deleted for *Slc20a2*, the most highly expressed Pi transporter in the tooth.

Material and Methods

Animals

Animal care and maintenance were provided through the University of Nantes accredited animal facility at the Unité de Thérapeutique Expérimentale. Mice were housed under specific pathogen-free conditions and were fed with RM1 diet for maintenance and with RM3 diet for breeding (SDS France). *Slc20a2*$^{tm1a(EUCOMM)Wtsi}$ mice (thereafter named *Slc20a2* KO mice) were obtained from the European Mouse Mutant Archive. The mutant allele contains an IRES:lacZ trapping cassette and a splicing site disrupting *Slc20a2* gene function and allowing the expression of the LacZ reporter (Skarnes et al. 2011). This study conformed to ARRIVE (Animal Research: Reporting of In Vivo Experiments) guidelines and was approved by the Animal Care Committee of Pays de la Loire (Apafis agreement 02286.02).

Patients

The human study protocol, consent form, and consent procedure were approved by the medical ethic committee of the University Hospital of Nantes (SVTO:DC-2011-1399). All patients were informed and gave their written consent to have their third molar extracted for research purpose. This protocol complied with the Code of Ethics of the World Medical Association (Declaration of Helsinki) and in agreement with ethical guidelines set by French law (bioethic law 2004-800).

Tissue Sample Processing

First mandibular molar germ isolations were performed as previously described (Nait Lechguer et al. 2008) from E14.5 to E18.5 embryos and P1 to P15 pups. Head samples for in situ hybridization and immunohistochemistry were harvested from C57BL/6 E12.5 to E18.5 embryos and P1 to P10 pups, fixed in 4% paraformaldehyde, decalcified in ethylenediaminetetraacetic acid (EDTA; 0.5 M, pH 8), and paraffin embedded. Resin-embedded samples (Technovit 9100 NEW, Kulzer) were used for histology. Human dental samples were harvested from patients needing extraction of impacted third molars or germectomy from Nolla stages 6 to 9.

Reverse Transcription and Real-time Polymerase Chain Reaction

To isolate RNA, human or mouse dental samples were crushed with a FastPrep system equipped with ceramic spheres in 0.5 mL of TRIzol (Life Technologies). The supernatant was then processed for nucleic acid purification with the Nucleospin RNA II Kit (Macherey-Nagel), according to the manufacturer's instructions. After quantification, 0.5 µg of RNA was reversed transcribed with SuperScriptIII (Life Technologies). Real-time polymerase chain reaction (PCR) was performed on Bio-Rad CFX96 with SYBRSelect Master Mix (Life Technologies). Primer efficiency was determined with a standard curve with a 1:4 dilution, and specificity of amplification was verified from the melting curve analysis. Target genes expression were normalized to *GusB* or *GAPDH* expression levels (Pfaffl 2001). Sequences of primers used in this study are listed in the Appendix Table.

In Situ Hybridization

Serial 5-µm-thick sections from paraffin-embedded tissues were processed for in situ hybridization (ISH) as previously described (Beck et al. 2010). All antisense and sense RNA probes (Appendix Table) were prepared by in vitro transcription from T7 or SP6 promoter (DIG RNA Labeling Kit; Roche). Deparaffinized sections were treated with proteinase K (5 µg/mL) for 15 min at 37 °C and incubated with 1-µg/mL labeled probe

overnight at 50 °C. After treatment with RNase A (20 µg/mL), labeled cells were visualized with DIG nucleic acid detection kit (Roche). Since the Slc20a1 signal was low, TSA amplification kit was used for this probe (Perkin Elmer). Sections were mounted in aqueous solution (Mowiol; Sigma) and scanned with a Hamamatsu NanoZoomer HT digital scanner (Hamamatsu Photonics KK).

Immunohistochemistry

Paraffin-embedded sections were processed for immunohistochemistry (IHC) as previously described (Beck et al. 2010). For Slc34a2 IHC, antigen retrieval was performed with 10mM citrate (pH 6, 20 min, 95 °C). Sections were then incubated overnight at 4 °C with polyclonal anti-Slc34a2 antibody (1:300) kindly provided by Pr Jurg Biber (University of Zurich; Traebert et al. 1999). Biotinylated goat anti-mouse secondary antibody (1:300; Dako) was used, and staining was performed with a diaminobenzidine chromogen. Osteopontin (OPN) and dentin sialoprotein (DSP) IHC was performed as previously described (Gaucher et al. 2009).

X-gal and Histologic Stainings

Tissue samples from 1-mo-old *Slc20a2* KO mice (carrying a LacZ allele) were fixed for 2 h at room temperature in 4% paraformaldehyde and incubated overnight at 32 °C in phosphate-buffered saline containing 0.01% Tween 20, 2mM $MgCl_2$, 4mM $K_4Fe(CN)_6$, and 1 mg/mL of X-gal. After postfixation, samples were decalcified in 0.5M EDTA (pH 8) for 1 to 3 wk at 4 °C, paraffin embedded, and sectioned (7 µm). For histologic staining, undecalcified resin-embedded samples were cut at 40-µm thickness with a diamond wire saw (Leitz) after ultraviolet glue fixation. Slices were treated 2 min with HCl 2% and then stained with methylene blue and basic fuchsin.

Micro–computed tomography

Three-dimensional x-ray acquisition of the samples was obtained with a SkyScan 1272, with the following acquisition parameters: pixel size, 7 to 13 µm; voltage, 90 kV; amperage, 100 µA; aluminum filter, 0.5 mm. The reconstruction was executed with NRecon software.

Statistics

Quantitative PCR (qPCR) experiments were repeated at least 3 times, and results were analyzed with analysis of variance. A total of 20 to 40 murine first mandibular molar germs were used for each developmental stage or age. Histologic measurements were analyzed with a Mann-Whitney test. qPCR data are expressed as mean ± SEM. A P value <0.05 was considered statistically significant.

Results

Expression of Pi Transporters during Tooth Development and Mineralization

The *Slc34a2* expression profile from E14.5 to P15 in murine tooth germs was biphasic, being strongly increased during postnatal stages, particularly after P6 (Fig. 1A). The expression of *Slc20a1* and *Slc20a2* was low during prenatal stages and increased after birth. However, while *Slc20a1* expression oscillated and remained relatively low, *Slc20a2* showed a continuous increase in expression, becoming significantly different after P6. *Slc20a2* was expressed at significantly higher levels than the other transporters, displaying 2- and 17-fold-higher expression than *Slc20a1* at E14.5 and P7, respectively (Fig. 1B). The expression of *Slc17a1* and *Slc34a3* was very low during the pre- and post-natal stages, being close to the detection limit of qPCR (Fig. 1B). *Slc34a1* expression did not vary significantly (not shown) and remained very weak as compared with *Slc34a2* and *Slc20a1* or, even more so, Slc20a2 (Fig. 1B). The expression profile of the Pi exporter *Xpr1* resembled the one of *Slc20a2*, although its expression was lower (Fig. 1A, B). These results show that the Pi transporters were weakly expressed during prenatal stages at the time of mineralization initiation (Appendix Fig. 1).

SLC17A1 expression in human tooth samples from Nolla stages 6 to 9 was undetectable, whereas *SLC34A2, SLC20A1, SLC20A2*, and *XPR1* were easily amplified (not shown). In contrast to the mice data, *SLC34A1* was undetectable in human tooth samples, whereas *SLC34A3* was readily detected (not shown). As with mice, *SLC20A2* was expressed at levels higher than those of the other transporters, displaying, for instance, a 87-fold-higher expression than *SLC20A1* at Nolla stage 6 (Fig. 1D).

Spatiotemporal Expression of Slc34a2, Slc20a1, and Slc20a2

To extend our data, we examined the localization of Pi transporter expression in teeth from wild-type mice. The specificity of ISH probes for *Slc17a1, Slc34a1, Slc34a2*, and *Slc34a3* were first tested on kidney sections from wild-type mice (Appendix Fig. 2A). Consistent with the reverse transcription qPCR results, no signal could be detected for *Slc17a1, Slc34a1*, and *Slc34a3* in dental and peripheral structures from E13.5 to P10 (not shown). Similarly, no signal could be detected with the *Slc34a2* ISH probe from E13.5 to P4 (Appendix Fig. 3A). However, at P10, a clear *Slc34a2* signal was visible in mature ameloblasts of the first and second molars (Fig. 2A), while no signal could be detected in odontoblasts at any investigated stage. Using a murine anti-Slc34a2 antibody that was validated on kidney histologic sections (Appendix Fig. 2B), we could detect the late expression of Slc34a2 in ameloblasts of the incisors (Fig. 2B) and molars (Appendix Fig. 3A) at P6 and P10.

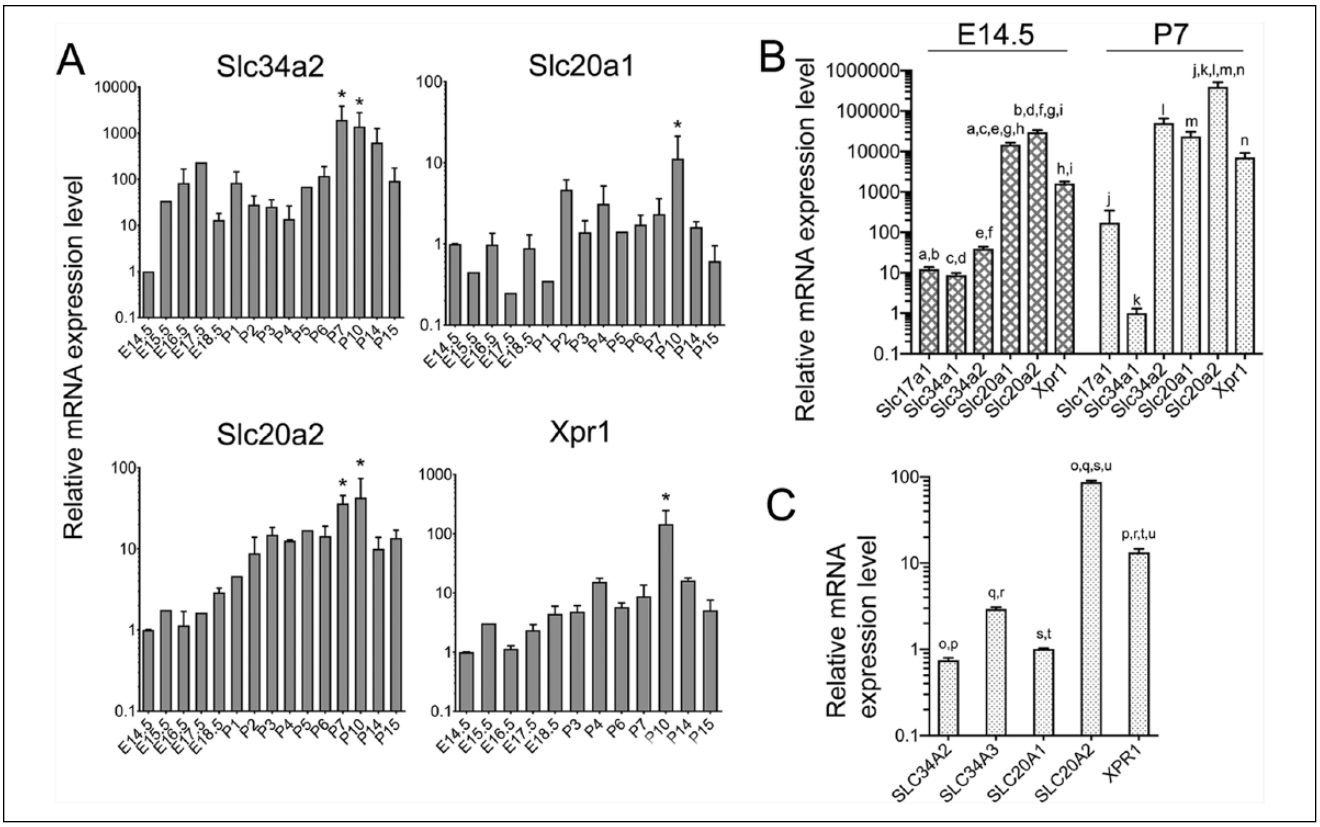

Figure 1. Expression of phosphate transporters during murine tooth development and mineralization. Molar germs were extracted from mice aged from embryonic day 14.5 (E14.5) to postnatal day 15 (P15); RNAs were extracted and reverse transcribed; and phosphate (Pi) transporter expressions were quantified by real-time polymerase chain reaction (PCR). (**A**) Relative RNA expression levels of *Slc34a2, Slc20a1, Slc20a2*, and *Xpr1* from E14.5 to P15 mandibular molar germs were determined by real-time PCR. The expression of *Slc17a1, Slc34a1*, and *Slc34a3* remained either very low or undetectable at any time point (not shown). Results were normalized with *GusB* as a reference gene and expressed relative to the expression level at E14.5 (set as 1). For each point, 20 to 40 murine tooth germs were used. *$P < 0.05$ versus expression level at E14.5. (**B**) Comparison of the RNA expression levels of Pi transporters at E14.5 and P7 in molar germs. The expression of Pi transporters was calculated relative to the expression of *Slc34a1* at P7, set as 1. Note that *Slc34a3* was not detected. Data are expressed as mean ± SEM. One-way analysis of variance, followed by Tukey's post hoc multiple comparison test, was used to compare expression levels within each developmental stage group (E14.5 or P7). Statistical differences between gene expression are indicated by paired letters. For instance, letter *a* indicates that *Slc17a1* and *Slc20a1* have a significantly different expression at E14.5. $P < 0.05$ for l, m; $P < 0.01$ for a, c, e, g, h, j, k, n; $P < 0.001$ for b, d, f, i. (**C**) Comparison of the RNA expression levels of Pi transporters at Nolla stage 6 in human molar germs. Third molar germs ($n = 9$) were removed surgically from patients ($n = 5$); RNA were extracted and reverse transcribed; and Na-Pi cotransporter expressions were quantified by real-time PCR. *SLC17A1* and *SLC34A1* expressions were undetectable at any stage (not shown). The expression of Pi transporters was calculated relative to the expression of *SLC20A1*, set as 1. Data are expressed as mean ± SEM. One-way analysis of variance, followed by Tukey's post hoc multiple comparison test, was used to compared expression levels. Statistical differences between gene expressions are indicated by paired letters. $P < 0.05$ for p, r, t; $P < 0.0001$ for o, q, s, u.

The expression pattern of Slc20a1 and Slc20a2, as investigated with available commercial antibodies by IHC, gave nonspecific signals that were similar between wild-type and KO animals (not shown). Consequently, we used an ISH approach and showed a strong positive ISH signal for *Slc20a1* in mature ameloblasts from incisors (Fig. 2C) and molars (Appendix Fig. 3B) at P6 and a fainter signal in adjacent secretory ameloblasts, with an absence of signal in odontoblasts. No *Slc20a1* ISH signal was obtained in tooth structures from embryonic stages (Appendix Fig. 3B). The *Slc20a2* localization expression in tooth was determined with the inserted LacZ reporter cassette of mutant mice. LacZ expression was absent from dental structures at any embryonic stage (not shown). However, a specific and intense LacZ signal was detected in the subodontoblastic layer (Hoehl cells) and in the stratum intermedium in vicinity of ameloblast epithelium from incisors and molars after birth (Fig. 2D; Appendix Fig. 3C). A specific and more diffuse signal was visible in the dental pulp mesenchyme. Importantly, ameloblasts, odontoblasts, and cementoblasts exhibited no LacZ signal (Fig. 2D; Appendix Fig. 3C) at any investigated stage or age.

In Vivo Involvement of Slc20a2 in Tooth Mineralization

Our data identified Slc20a2 as the most significantly expressed Pi transporter in tooth germs. Surprisingly, Slc20a2 was not expressed in mineralizing cells but rather in adjacent cells. To

determine the physiologic relevance of these observations, we examined the histologic phenotype of teeth from *Slc20a2*-deficient mice. The enamel thickness and aspect were similar between wild-type and *Slc20a2* KO mice at 1 mo (Fig. 3A, B) and 8 mo (Fig. 3C, D) of age. The aspect of the ameloblast palisade appeared similar between the 2 mice at both ages (Fig. 3E–H). However, the thickness of the predentin layer increased in young and old mutant mice, whereas the thickness of the dentin layer decreased (Fig. 3A–D, Table; Appendix Fig. 4C). However, the total thickness of the 2 layers remained similar (Table). Interestingly, the mineralization front between the predentin and dentin layers exhibited excessive unmerged calcospherites (Fig. 3J, L). The predentin/dentin phenotype did not improve with age between young and old animals. No histologic differences were seen in the cementum between mutant and control mice (Fig. 3M–P).

The expression of DSP and OPN was detected as expected in predentin nearby odontoblasts (Fig. 4A–D) and in abnormal interglobular spaces of *Slc20a2*-deficient dentin sections. DSP staining usually found in dentin tubules was maintained in mutant mice (Fig. 4B, D).

Discussion

In this study, we provided an exhaustive spatiotemporal information on Pi transporter expression in tooth. We obtained these data in a model of tooth germs, which preserves the spatial organization

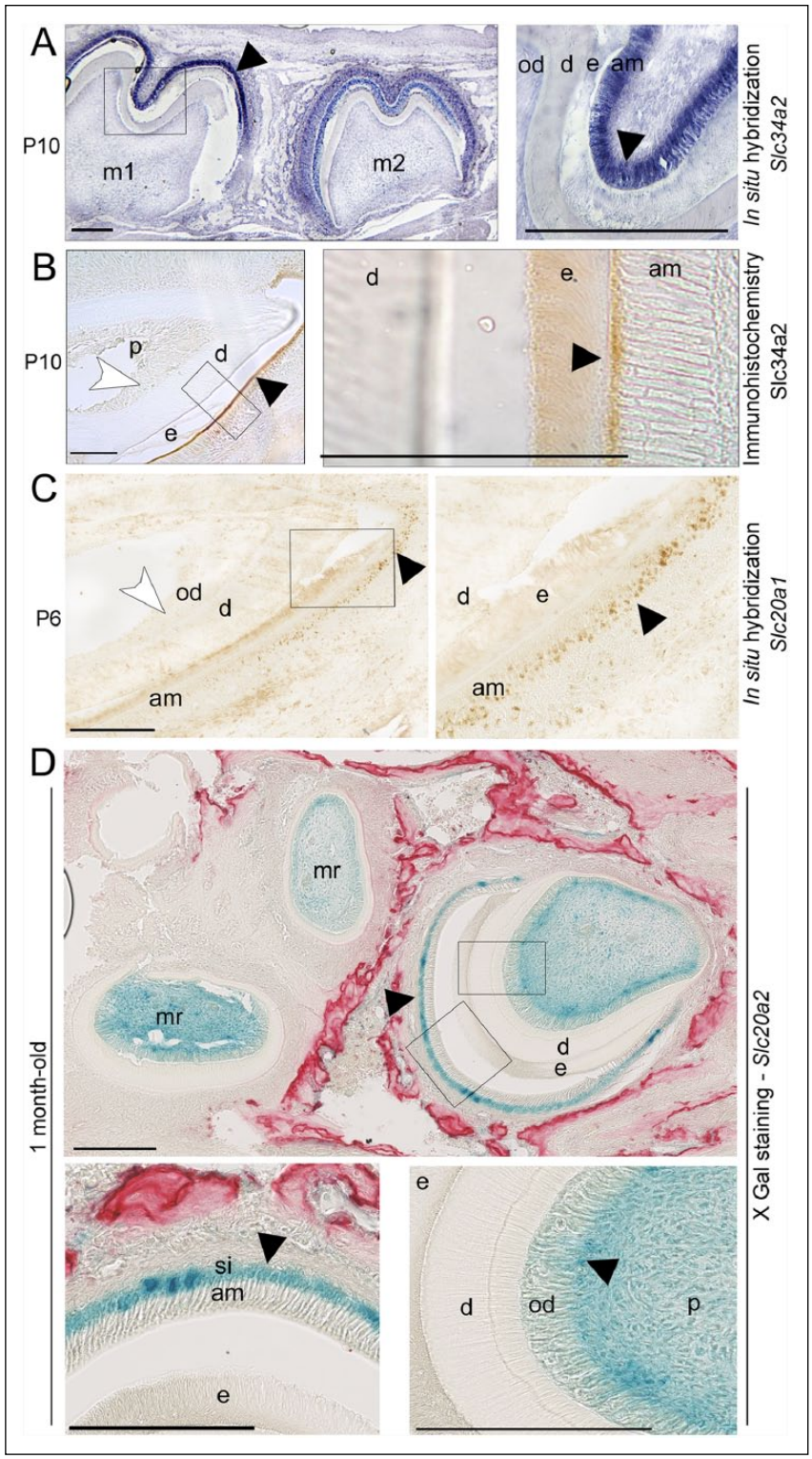

Figure 2. Spatiotemporal expression of *Slc34a2, Slc20a1*, and *Slc20a2* during dental development. Head samples were harvested from C57BL/6J wild-type embryos or pups, decalcified, and paraffin embedded prior to in situ hybridization (ISH) and immunohistochemistry (IHC). (**A**) ISH with an *Slc34a2* probe showed an intense signal in mature ameloblasts of the first mandibular molar at postnatal day 10 (P10; black arrowhead). A higher magnification is shown on the right panel. A weaker signal is obtained in secretory ameloblasts of the second molar. Bar = 100 µm. (**B**) Slc34a2 IHC in mouse incisor at P10: note the specific signal (black arrowhead) visible in the ameloblasts and the absence of signal in the odontoblasts (white arrowhead) or in any other dental cells. A higher magnification is shown on the right panel. Bar = 100 µm. (**C**) *Slc20a1* ISH in the incisor of P6 mouse pups with a TSA amplification kit revealing a specific *Slc20a1* signal in mature ameloblasts and a weaker signal in secretory ameloblasts (black arrowheads). No signal was detected in odontoblasts (white arrowhead). Bar = 250 µm. (**D**) X-gal stainings of 1-mo-old paraffin-embedded *Slc20a2* KO incisors. The strongest staining was observed in the stratum intermedium and subodontoblastic layer (black arrowhead); a more diffuse signal in the pulp was observed; and no signal could be seen in the cementoblasts. Bar = 250 µm. am, ameloblasts; d, dentin; e, enamel; m1, first molar; m2, second molar; mr, molar root; od, odontoblasts; p, pulp; si, stratum intermedium.

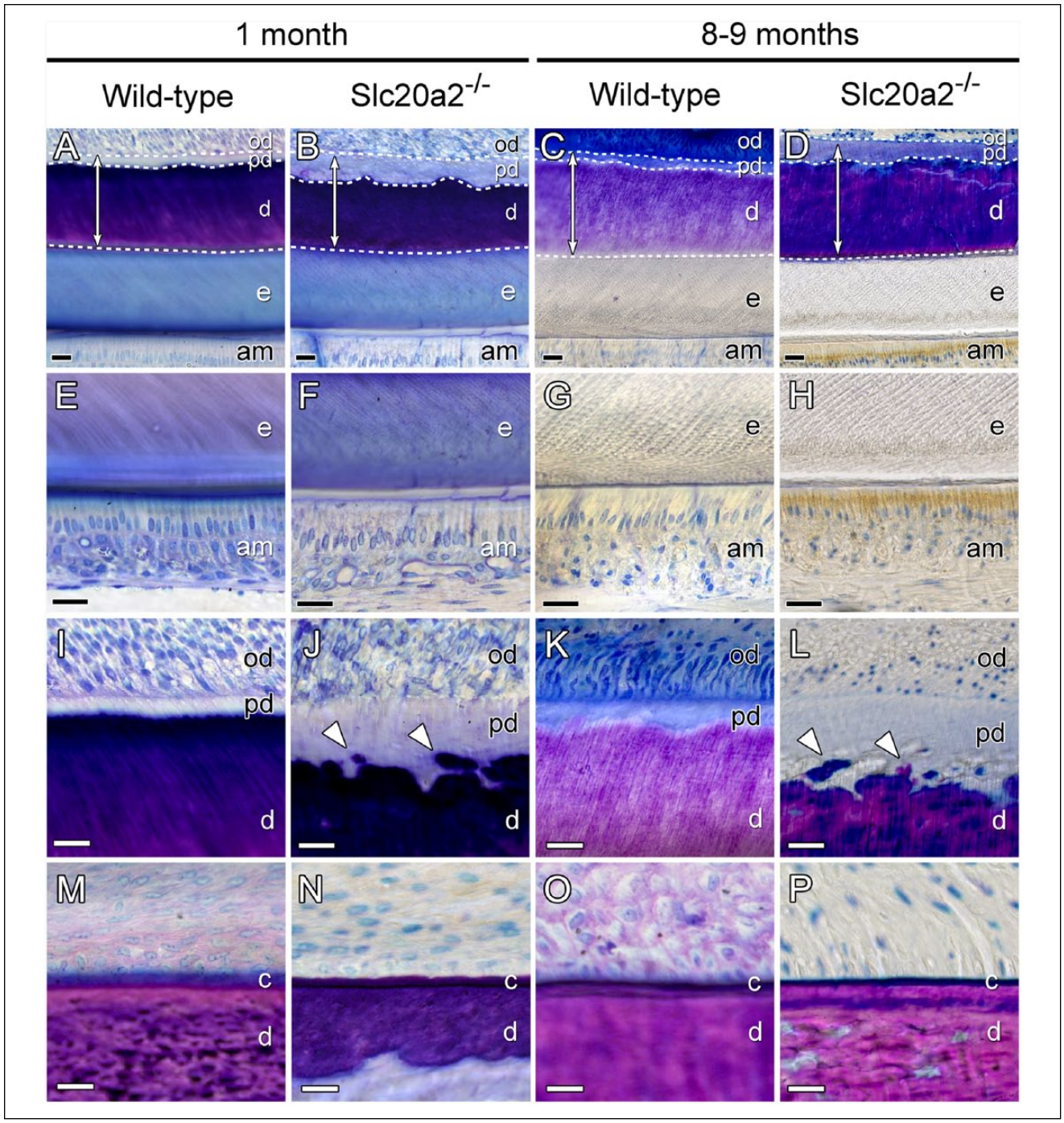

Figure 3. *Slc20a2*-deficient mice display an abnormal dentinogenesis. Incisors from 1- and 9-mo-old wild-type and *Slc20a2* KO mice were resin embedded and cut into 70-µm-thick slices, which were then stained with toluidine blue and red fuchsin. (**A–D**) An enlarged predentin layer is visible in *Slc20a2* KO mice at both ages, with no major modification of the total thickness of the combined predentin-dentin layer (arrows) or the enamel layer. (**E–H**) At both ages, the ameloblast layer of *Slc20a2* KO animals did not show significant differences. (**I–L**) At higher magnification, the examination of the predentin layer of mutant mice revealed the presence of calcospherites (arrowheads). (**M–P**) No obvious difference could be observed in the cementum layer of mutant *Slc20a2* mice when compared with wild-type mice. Bar = 25 µm. am, ameloblasts; d, dentin; e, enamel; od, odontoblasts; pd, predentin.

of the tooth, the epithelial-mesenchymal interactions, and the diversity of tooth cell types. Our most striking findings is that none of the transporters were expressed at a high level at the time of mineralization initiation. This is in contrast with current hypotheses establishing that Pi transporters would necessarily be expressed in mineralizing cells during this crucial step to provide enough Pi for the nucleation and growth of hydroxyapatite crystals. Rather, we showed that the expression of Pi

Table. Thickness of Dentin and Predentin Layers from Incisors of Wild-Type and *Slc20a2*$^{-/-}$ Mutant Mice.

	1 mo Old		9 mo Old	
Histologic Measurement	Wild Type	*Slc20a2*$^{-/-}$	Wild Type	*Slc20a2*$^{-/-}$
Thickness, µm				
Mineralized dentin	134.56 ± 12.65	104.60 ± 19.52[a]	187.66 ± 23.12	94.01 ± 4.39[b]
Predentin	7.99 ± 1.97	35.50 ± 8.87[b]	16.26 ± 1.95	73.95 ± 2.47[b]
Overall dentin	142.55 ± 11.09	140.10 ± 27.31, NS	203.93 ± 21.54	167.96 ± 6.62[a]
Ratio: predentin:mineralized dentin	0.06 ± 0.01	0.34 ± 0.04[b]	0.09 ± 0.02	0.79 ± 0.02[b]

NS, not significant.
[a]$P < 0.05$ (*Slc20a2*$^{-/-}$ vs. wild-type mice).
[b]$P < 0.001$ (*Slc20a2*$^{-/-}$ vs. wild-type mice).

transporters peaked long after the initiation of dentin or enamel mineralization. This suggests that while they can still be important for some aspects of tooth mineralization (e.g., the maturation phase), the currently known Pi transporters are likely dispensable for the initiation of tooth mineralization.

Although a thorough dental phenotypic analysis has not been performed in the hypomorphic *Slc20a1* mice (Bourgine et al. 2013) and *DMP1-Cre;Slc20a1*$^{lox/lox}$ mice, we could not evidence major dental abnormalities in these mice, reinforcing the idea that Slc20a1 is not mandatory for the initiation of dental mineralization. Similarly, no obvious dental phenotype has been reported in *Slc34a1* KO mice (Beck et al. 1998), consistent with the faint expression of *Slc34a1* in mouse germs and its absence from human samples (Onishi et al. 2007; Tada et al. 2011; Merametdjian et al. 2016).

In humans, mutation or deletion of the SLC34A3 gene is responsible for hereditary hypophosphatemic rickets with hypercalciuria (Bergwitz et al. 2006; Ichikawa et al. 2006; Lorenz-Depiereux et al. 2006). Similar inherited disorders of Pi wasting, such as X-linked hypophosphatemic rickets (XLH) or autosomal dominant hypophosphatemic rickets (ADHR), display poorly mineralized teeth, including enamel hypoplasia with a default of the formation of hydroxyapatite crystals and the presence of interglobular dentin originating from insufficient fusion of calcospherites (Opsahl Vital et al. 2012; Foster et al. 2014). However, no similar observations were reported for patients with hereditary hypophosphatemic rickets with hypercalciuria. In addition, Slc34a3 has been characterized as a transporter having low Pi transport and concentrating capacities (Virkki et al. 2007). Therefore, its very faint expression and poor Pi transport properties make this transporter an inadequate candidate to face the Pi needs required for tooth mineralization.

We identified Slc20a2 as being the most highly expressed Pi cotransporter in the tooth and demonstrated that absence of Slc20a2 in mice led to a dentin dysplasia resembling the tooth phenotype of patients with XLH and ADHR and *Dspp*$^{-/-}$ mice (Sreenath et al. 2003; Gaucher et al. 2009). Strikingly, while patients with XLH and ADHR and *Dspp* KO mice are hypophosphatemic, the *Slc20a2* KO mouse is normophosphatemic (Jensen et al. 2016; Wallingford et al. 2017). At first sight, it seems difficult to explain the similar tooth phenotypes arising from different gene mutations on the sole basis of Pi serum levels. It is possible that the local extracellular Pi level, rather than

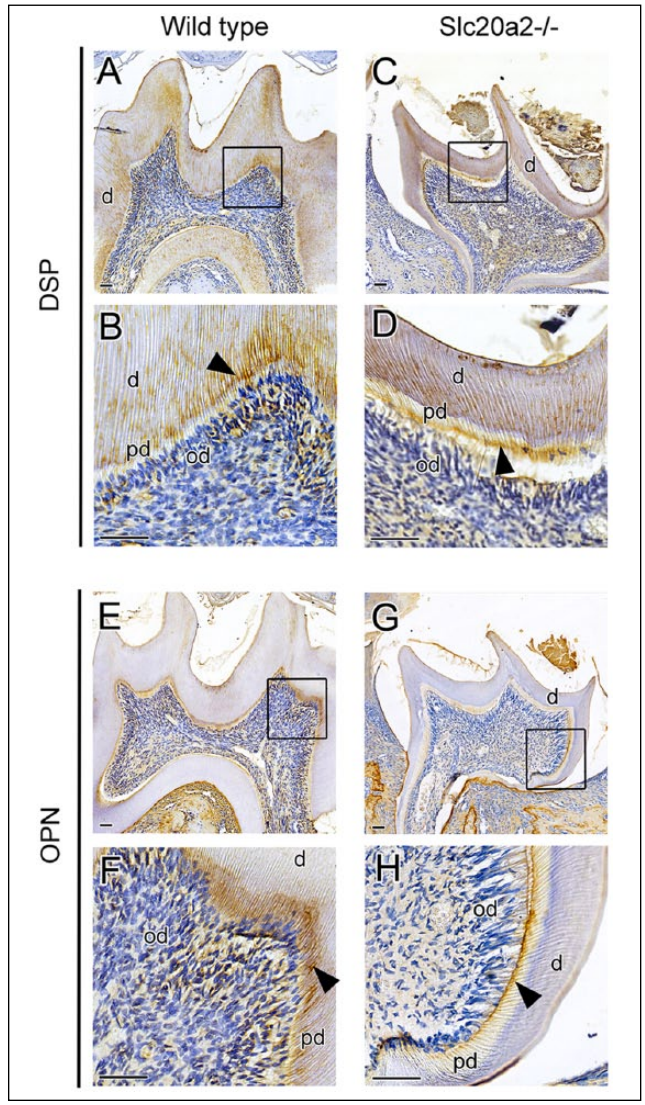

Figure 4. Dentin sialoprotein (DSP) and osteopontin (OPN) expression is normal in *Slc20a2*-deficient teeth. Molars from 1-mo-old wild-type and *Slc20a2* KO mice were decalcified and paraffin embedded before processing to immunohistochemistry (IHC). (**A–D**) DSP IHC revealed no obvious difference between wild-type and *Slc20a2*-deficient animals. DSP signal is shown (black arrowheads). (**E–H**) Similarly, OPN IHC was detected at the secretary pole of odontoblasts and predentin layer in both wild-type and *Slc20a2*-deficient teeth (black arrowheads). Bar = 50 µm. d, dentin; od, odontoblasts; pd, predentin.

the serum Pi levels, may be a key factor in the etiology of the shared phenotype. Interestingly, *SLC20A2* mutations in humans were shown to be causative of idiopathic basal ganglia calcification, characterized by calcium/Pi deposits predominantly located within the walls of small arteries and veins (Wang et al. 2012). The absence of SLC20A2 in the vascular epithelium precludes Pi to reach the extracellular compartment, which then accumulates within the vessels. Hence, a deficiency in Pi uptake due to Slc20a2 deficiency could result in a decrease in local Pi availability in the vicinity of mineralizing cells leading to a phenotype similar to hypophosphatemic conditions.

Overall, our data call into question the role of the currently known Pi transporters in mineralizing dental cells. Their expression profile and levels and the phenotypes associated with Pi transporter defects do not support a major role of these transporters in the initiation of dental mineralization. In addition, the quantities of Pi needed for mineralization are at odds with the low transporting capacity of these transporters. Other Pi transporters displaying weaker affinities for Pi but higher transport capacities may exist in bone, as described earlier for renal cells (Walker et al. 1987; Tenenhouse et al. 1989). Being expressed at later stages, the high-affinity Pi transporters may rather participate, directly or indirectly, to the regulation and maintenance of tooth mineralization throughout the life span. An interesting possibility is that the Pi transporters may be part of a Pi sensing and signaling pathway in mineralizing cells, as suggested >15 y ago (Beck et al. 2000). This hypothesis is consistent with the high affinity of the transporters for Pi, as well as recent observations (Chavkin et al. 2015) illustrating their role in Pi signaling. This possible role of the high-affinity Pi transporters in mediating Pi signaling in teeth is consistent with our most singular finding describing high levels of *Slc20a2* expression in the stratum intermedium, the subodontoblastic layer of Hoehl cells, and the pulp, which are not mineralizing cells but are located in their close proximity.

In summary, by documenting the spatiotemporal expression of high-affinity Pi transporters in the tooth, our study supports the notion that none of the currently identified high-affinity Pi transporters are mandatory for the initiation of mineralization. Clearly, further work is needed to decipher their role in tooth mineralization during aging and to identify other putative Pi transport systems at work.

Author Contributions

L. Merametdjian, C. Gaucher, L. Beck, contributed to conception, design, and data analysis, drafted and critically revised the manuscript; S. Beck-Cormier, contributed to conception, design, and data analysis, critically revised the manuscript; N. Bon, G. Couasnay, S. Source, contributed to conception and design, critically revised the manuscript; J. Guicheux, contributed to data analysis, critically revised the manuscript.

Acknowledgments

This work was supported by INSERM, Université de Nantes, Région Pays de Loire, IFRO, and CHU de Nantes. We gratefully thank Frederic Lezot for his helpful advice; the team of Hervé Lesot (INSERM UMR 1109, Strasbourg, France), particularly Laetitia Keller and Tunay Kokten, for teaching the tooth germ dissection technique; and Constance Artus, Mathilde Mangel, and Julie Lesieur for their contribution to histologic work. We thank Drs. Philippe Lesclous and Alexandra Cloitre for providing human tooth samples. The authors declare no potential conflicts of interest with respect to the authorship and/or publication of this article.

References

Beck G, Zerler B, Moran E. Phosphate is a specific signal for induction of osteopontin gene expression. 2000. Proc Natl Acad Sci U S A. 97(15):8352–8357.

Beck L, Karaplis AC, Amizuka N, Hewson AS, Ozawa H, Tenenhouse HS. 1998. Targeted inactivation of Npt2 in mice leads to severe renal phosphate wasting, hypercalciuria, and skeletal abnormalities. Proc Natl Acad Sci U S A. 95(9):5372–5377.

Beck L, Leroy C, Beck-Cormier S, Forand A, Salaun C, Paris N, Bernier A, Urena-Torres P, Prie D, Ollero M, et al. 2010. The phosphate transporter PiT1 (Slc20a1) revealed as a new essential gene for mouse liver development. PloS One. 5(2):e9148.

Bergwitz C, Roslin NM, Tieder M, Loredo-Osti JC, Bastepe M, Abu-Zahra H, Frappier D, Burkett K, Carpenter TO, Anderson D, et al. 2006. SLC34A3 mutations in patients with hereditary hypophosphatemic rickets with hypercalciuria predict a key role for the sodium-phosphate cotransporter NaPi-IIc in maintaining phosphate homeostasis. Am J Hum Genet. 78(2):179–192.

Boonrungsiman S, Gentleman E, Carzaniga R, Evans ND, McComb DW, Porter AE, Stevens MM. 2012. The role of intracellular calcium phosphate in osteoblast-mediated bone apatite formation. Proc Natl Acad Sci U S A. 109(35):14170–14175.

Bourgine A, Beck L, Khoshniat S, Wauquier F, Oliver L, Hue E, Alliot-Licht B, Weiss P, Guicheux J, Wittrant Y. 2011. Inorganic phosphate stimulates apoptosis in murine MO6-G3 odontoblast-like cells. Arch Oral Biol. 56(10):977–983.

Bourgine A, Pilet P, Diouani S, Source S, Lesoeur J, Beck-Cormier S, Khoshniat S, Weiss P, Friedlander G, Guicheux J, et al. 2013. Mice with hypomorphic expression of the sodium-phosphate cotransporter PiT1/Slc20a1 have an unexpected normal bone mineralization. PloS One. 8(6):e65979.

Chavkin NW, Chia JJ, Crouthamel MH, Giachelli CM. 2015. Phosphate uptake-independent signaling functions of the type III sodium-dependent phosphate transporter, PiT-1, in vascular smooth muscle cells. Exp Cell Res. 333(1):39–48.

Forster I, Hernando N, Sorribas V, Werner A. 2011. Phosphate transporters in renal, gastrointestinal, and other tissues. Adv Chronic Kidney Dis. 18(2):63–76.

Foster BL, Nociti FH Jr, Somerman MJ. 2014. The rachitic tooth. Endocrine Rev. 35(1):1–34.

Gaucher C, Boukpessi T, Septier D, Jehan F, Rowe PS, Garabedian M, Goldberg M, Chaussain-Miller C. 2009. Dentin noncollagenous matrix proteins in familial hypophosphatemic rickets. Cells Tissues Organs. 189(1–4):219–223.

Habraken WJ, Tao J, Brylka LJ, Friedrich H, Bertinetti L, Schenk AS, Verch A, Dmitrovic V, Bomans PH, Frederik PM, et al. 2013. Ion-association complexes unite classical and non-classical theories for the biomimetic nucleation of calcium phosphate. Nat Commun. 4:1507.

Ichikawa S, Sorenson AH, Imel EA, Friedman NE, Gertner JM, Econs MJ. 2006. Intronic deletions in the SLC34A3 gene cause hereditary hypophosphatemic rickets with hypercalciuria. J Clin Endocrinol Metab. 91(10):4022–4027.

Jensen N, Autzen JK, Pedersen L. 2016. Slc20a2 is critical for maintaining a physiologic inorganic phosphate level in cerebrospinal fluid. Neurogenetics. 17(2):125–130.

Lorenz-Depiereux B, Benet-Pages A, Eckstein G, Tenenbaum-Rakover Y, Wagenstaller J, Tiosano D, Gershoni-Baruch R, Albers N, Lichtner P, Schnabel D, et al. 2006. Hereditary hypophosphatemic rickets with hypercalciuria is caused by mutations in the sodium-phosphate cotransporter gene SLC34A3. Am J Hum Genet. 78(2):193–201.

Lundquist P, Ritchie HH, Moore K, Lundgren T, Linde A. 2002. Phosphate and calcium uptake by rat odontoblast-like MRPC-1 cells concomitant with mineralization. J Bone Miner Res. 17(10):1801–1813.

Merametdjian L, David A, Bon N, Couasnay G, Guicheux J, Gaucher C, Beck-Cormier S, Beck L. 2016. Expression of phosphate transporters in optimized cell culture models for dental cells biomineralization. Bull Group Int Rech Sci Stomatol Odontol. 53(1):e16.

Millán JL. 2013. The role of phosphatases in the initiation of skeletal mineralization. Calcif Tissue Int. 93(4):299–306.

Nait Lechguer A, Kuchler-Bopp S, Hu B, Haikel Y, Lesot H. 2008. Vascularization of engineered teeth. J Dent Res. 87(12):1138–1143.

Onishi T, Okawa R, Ogawa T, Shintani S, Ooshima T. 2007. Phex mutation causes the reduction of npt2b mRNA in teeth. J Dent Res. 86(2):158–162.

Opsahl Vital S, Gaucher C, Bardet C, Rowe PS, George A, Linglart A, Chaussain C. 2012. Tooth dentin defects reflect genetic disorders affecting bone mineralization. Bone. 50(4):989–997.

Pfaffl MW. 2001. A new mathematical model for relative quantification in real-time RT-PCR. Nucleic Acids Res. 29(9):e45.

Reimer RJ. 2013. Slc17: a functionally diverse family of organic anion transporters. Mol Aspects Med. 34(2–3):350–359.

Skarnes WC, Rosen B, West AP, Koutsourakis M, Bushell W, Iyer V, Mujica AO, Thomas M, Harrow J, Cox T, et al. 2011. A conditional knockout resource for the genome-wide study of mouse gene function. Nature. 474(7351):337–342.

Sreenath T, Thyagarajan T, Hall B, Longenecker G, D'Souza R, Hong S, Wright JT, MacDougall M, Sauk J, Kulkarni AB. 2003. Dentin sialophosphoprotein knockout mouse teeth display widened predentin zone and develop defective dentin mineralization similar to human dentinogenesis imperfecta type III. J Biol Chem. 278(27):24874–24880.

Tada H, Nemoto E, Foster BL, Somerman MJ, Shimauchi H. 2011. Phosphate increases bone morphogenetic protein-2 expression through cAMP-dependent protein kinase and ERK1/2 pathways in human dental pulp cells. Bone. 48(6):1409–1416.

Tenenhouse HS, Klugerman AH, Neal JL. 1989. Effect of phosphonoformic acid, dietary phosphate and the Hyp mutation on kinetically distinct phosphate transport processes in mouse kidney. Biochim Biophys Acta. 984(2):207–213.

Traebert M, Hattenhauer O, Murer H, Kaissling B, Biber J. 1999. Expression of type II Na-P(i) cotransporter in alveolar type II cells. Am J Physiol. 277(5 Pt 1):L868–L873.

Veis A, Dorvee JR. 2013. Biomineralization mechanisms: a new paradigm for crystal nucleation in organic matrices. Calcif Tissue Int. 93(4):307–315.

Virkki LV, Biber J, Murer H, Forster IC. 2007. Phosphate transporters: a tale of two solute carrier families. Am J Physiol Renal Physiol. 293(3):F643–F654.

Walker JJ, Yan TS, Quamme GA. 1987. Presence of multiple sodium-dependent phosphate transport processes in proximal brush-border membrane. Am J Physiol. 252(2 Pt 2):F226–F231.

Wallingford MC, Chia JJ, Leaf EM, Borgeia S, Chavkin NW, Sawangmake C, Marro K, Cox TC, Speer MY, Giachelli CM. 2017. SLC20A2 deficiency in mice leads to elevated phosphate levels in cerbrospinal fluid and glymphatic pathway-associated arteriolar calcification, and recapitulates human idiopathic basal ganglia calcification. Brain Pathol. 27(1):64–76.

Wang C, Li Y, Shi L, Ren J, Patti M, Wang T, de Oliveira JR, Sobrido MJ, Quintans B, Baquero M, et al. 2012. Mutations in SLC20A2 link familial idiopathic basal ganglia calcification with phosphate homeostasis. Nature Genet. 44(3):254–256.

Wittrant Y, Bourgine A, Khoshniat S, Alliot-Licht B, Masson M, Gatius M, Rouillon T, Weiss P, Beck L, Guicheux J. 2009. Inorganic phosphate regulates Glvr-1 and -2 expression: role of calcium and ERK1/2. Biochem Biophys Res Commun. 381(2):259–263.

Yoshioka H, Yoshiko Y, Minamizaki T, Suzuki S, Koma Y, Nobukiyo A, Sotomaru Y, Suzuki A, Itoh M, Maeda N. 2011. Incisor enamel formation is impaired in transgenic rats overexpressing the type III NaPi transporter Slc20a1. Calcif Tissue Int. 89(3):192–202.

Zhao D, Vaziri Sani F, Nilsson J, Rodenburg M, Stocking C, Linde A, Gritli-Linde A. 2006. Expression of Pit2 sodium-phosphate cotransporter during murine odontogenesis is developmentally regulated. Eur J Oral Sci. 114(6):517–523.